Published in final edited form as:
Neuroimage. 2013 February 1; 0: 203–214. doi:10.1016/j.neuroimage.2012.10.090.

Genetic effects on behavior are mediated by neurotransmitters and large-scale neural networks

Linh C. Dang[1,2], **James P. O'Neil**[2], and **William J. Jagust**[1,2,3]

[1]Helen Wills Neuroscience Institute, University of California, Berkeley 132 Barker Hall #3190, Berkeley, CA 94720-3190

[2]Lawrence Berkeley National Laboratory 1 Cyclotron Road 55R0121, Berkeley, CA 94720-8119

[3]School of Public Health, University of California, Berkeley

Abstract

Claims of gene-behavior associations are complex and sometimes difficult to replicate because these relationships involve many downstream endogenous and environmental processes that mediate genetic effects. Knowing these mediating processes is critical to understanding the links between genes and behavior and how these factors differ between people. We identified and characterized the effects of a gene on neurochemistry and neural networks to elucidate the mechanism, at the systems level, whereby genes influence cognition. Catechol-O-methyltransferase (COMT) degrades dopamine in the prefrontal cortex (PFC) and is polymorphic with alleles differing in enzymatic activity. We found that COMT genotype determined dopamine synthesis, such that individuals with greater COMT activity synthesized more dopamine. Dopamine synthesis in the midbrain and ventral striatum affected functional connectivity in the default mode network, likely through the mesocorticolimbic pathway, in an inverted-U pattern with greater functional connectivity in medial PFC associated with intermediate levels of COMT activity and dopamine. Greater functional connectivity correlated with greater deactivation during performance of a set-shifting task that engaged the PFC. Greater deactivation was in turn associated with better performance. The integration of these results yields a model whereby COMT affects prefrontal function by a mechanism involving dopaminergic modulation of the default mode network. The model features the well-known inverted-U function between dopamine and performance and supports the hypothesis that dopamine and the default mode network shift attentional resources to influence prefrontal cognition.

Corresponding author: Linh C. Dang Helen Wills Neuroscience Institute 132 Barker Hall #3190 Berkeley, CA 94720-3190 Phone: (510) 643-6616 linhdang@berkeley.edu.
Authors' emails:
Linh C. Dang: linhdang@berkeley.edu
James P. O'Neil: jponeil@lbl.gov
William J. Jagust: jagust@berkeley.edu

Keywords

COMT; dopamine; prefrontal cortex; default mode network; set shifting

1. Introduction

Dopamine is critical for cognitive functions involving the prefrontal cortex (PFC) (Braver and Cohen, 2000). Catechol-O-methyltransferase (COMT) degrades dopamine in the PFC (Dickinson and Elvevag, 2009). A nucleotide substitution in the COMT gene replaces a valine (Val) with a methionine (Met), resulting in a less active enzyme that quadruples the concentration of dopamine in the PFC (Lachman et al., 1996). Studies relating COMT genotype to prefrontal function yield conflicting results (Egan et al., 2001; Mattay et al., 2003), demonstrating that a direct correlation between gene and behavior reflects a partial relationship that is unstable without knowledge of the mechanism of COMT function.

The immediate function of COMT in the PFC is dopamine degradation, suggesting that COMT modulates neural activity and cognition via dopamine activity. Human autopsy studies found an association between the Val allele and increased expression of a dopamine-synthesizing enzyme (Akil et al., 2003). We therefore used positron emission tomography (PET) to measure dopamine synthesis capacity *in vivo* to assess the influence of COMT polymorphism on dopamine activity.

Dopamine may affect cognition by facilitating neuronal synchrony. Local field potential recordings showed that dopamine modulates oscillations in the γ-band proposed to support cortical activity relating to perceptual and cognitive performance (Sharott et al., 2005; Ward, 2003). Neuronal synchrony may be the cellular basis of temporal coherence seen with functional magnetic resonance imaging (fMRI). Without an externally driven task, brain activity seen with fMRI fluctuates in coherent patterns called resting state networks (RSNs) (Biswal et al., 1995). RSNs are thought to reflect functional systems involved in cognitive processes (De Luca et al., 2006). Similar to γ-band oscillations, temporal coherence within RSNs, known as functional connectivity, decreases after dopamine depletion (Nagano-Saito et al., 2008). We therefore acquired fMRI signal in the absence of a task and related these to our PET measures of dopamine to assess the role of this neurotransmitter in modulating functional connectivity in RSNs.

RSNs may arise from the “idling state” of functional networks and can be predictive of task-induced fMRI activity (De Luca et al., 2006; Mennes et al., 2010). We acquired fMRI signal during performance of a prefrontal function task to explore the relationship between resting state and task-related activity. A prefrontal function associated with COMT and dopamine is cognitive flexibility, or the ability to change behavior in response to relevant changes in the environment (Cools et al., 2001; Nolan et al., 2004). Setshift tasks probe cognitive flexibility by assessing the subject's response as the rule of the task changes unpredictably (Monchi et al., 2004). We hypothesized that individual differences in setshift performance would relate to fMRI activity during task performance and, indirectly, functional connectivity in RSNs and dopamine function.

Lastly, we propose a model of how COMT influences prefrontal cognition through dopamine synthesis, resting state fMRI activity, and task-related fMRI activity. A complex multimodal assessment of this sort will be necessary for a full understanding of the relationships between genetics and behavior that will improve prediction of genetic effects on behavior and their role in disease.

2. Materials and Methods

2.1 Subjects

Fifteen right-handed, young adults between 20 and 30 years old (mean age 25.3 ± 2.8 years, 8M/7F) were recruited via flyers and online postings. Subjects were excluded if they had a Mini Mental State Exam (Folstein et al., 1975) score less than 28, a known major systemic disease, a history of psychiatric or neurological disorder, a history of substance abuse, current usage of medication known to affect dopaminergic or any neurological function, current or prior symptoms of depression, a serious head injury, or any contraindications to MR imaging. Subjects gave written informed consent prior to undergoing a PET scan with 6-[^{18}F]fluoro-l-m-tyrosine (FMT), a resting state fMRI scan, task-related fMRI scans, and genotyping. The current study was approved by institutional review boards at University of California, Berkeley and Lawrence Berkeley National Laboratory.

2.2 Genotype

Blood samples were collected from subjects and stored at the DNA Bank at the University of California, San Francisco (UCSF). UCSF's Genetics Core Facility performed COMT genotyping (Lachman et al., 1996). Of the fifteen subjects, 5 were met/met, 4 were met/val, and 6 were val/val.

2.3 PET data acquisition

PET imaging and FMT synthesis were performed at Lawrence Berkeley National Laboratory. FMT synthesis has been described previously (VanBrocklin et al., 2004). FMT is a substrate of aromatic L-amino acid decarboxylase (AADC), a dopamine-synthesizing enzyme whose activity provides an estimate of the ability of dopaminergic neurons to synthesize dopamine when provided with optimal substrate (DeJesus, 2003). FMT is metabolized by AADC to 6-[^{18}F]fluorometatyramine, which is oxidized to 6-[^{18}F]fluorohydroxyphenylacetic acid (FPAC). FPAC is visible on PET-FMT scans. Signal intensity on PET-FMT scans is thus indicative of dopamine synthesis capacity.

Subjects received an oral dose of carbidopa (2.5mg/kg) approximately 60 minutes before FMT injection. Carbidopa inhibits peripheral decarboxylation of FMT, resulting in a higher PET signal. Carbidopa does not cross the blood brain barrier (Clark et al., 1973) and has no detectable clinical effects in the dose range used in this study.

PET scans were acquired on a Siemens ECAT-HR PET camera with a 3.6-mm in-plane spatial resolution, 47 parallel imaging planes, and retractable septae for 3D imaging. Subjects were positioned in the scanner for a 10-min transmission scan used for attenuation correction. Following the scan, approximately 2.5 mCi of FMT was injected as a bolus into

an antecubital vein. Eighty-nine minutes of dynamic acquisition was acquired in the following sequence of frames: 4 × 60s, 3 × 120s, 3 × 180s, and 14 × 300s. FMT images were reconstructed with an ordered subset expectation maximization algorithm with weighted attenuation, scatter corrected, and smoothed with a 4mm full width half maximum kernel.

2.4 Regions of interest (ROIs)

We drew ROIs by visual inspection on each subject's mean MPRAGE MRI scan using FSLview. Dorsal caudate, dorsal putamen, and ventral striatum ROIs were drawn according to previously published guidelines (Mawlawi et al., 2001). Midbrain ROIs were drawn on five consecutive axial slices, the most caudal being the slice on which frontopontine fibers were separated into left and right bundles and the substantia nigra was clearly outlined (Fig. 1A). Both intrarater and interrater reliability were greater than 95%. The cerebellum grey matter was the reference region for calculating PET-FMT values. Because the cerebellum is located posterior and adjacent to the midbrain, limited PET spatial resolution introduces blurring and causes signal to spill onto neighboring regions. To avoid contamination of FMT signal from the midbrain, only the posterior ¾ of the cerebellum was included in the ROI.

2.5 PET data analysis

FMT frames were realigned to the middle frame, the twelfth frame, to correct for movement during scanning. ROIs were mapped to FMT space using the matrix calculated by FSL-FLIRT for coregistering the mean MPRAGE to the mean image of the realigned FMT frames (http://www.fmrib.ox.ac.uk/fsl/, version 4.1.2). After coregistration, ROI masks were thresholded at 0.5 to ensure high tissue probability. An in-house graphical analysis program implementing Patlak plotting (Patlak and Blasberg, 1985) with the cerebellum as the reference region created K_i images (Fig. 1A), which represent the amount of tracer accumulated in the brain relative to the cerebellum and are comparable to K_i images obtained using a blood input function but scaled to the volume of distribution of the tracer in the cerebellar reference region. K_i values from the ROIs were extracted.

2.6 MRI data acquisition

MRI data were acquired on a Siemens 1.5T Magnetom Avanto System with a 12-channel head coil. Foam cushions and headphones were provided to enhance comfort and reduce head movement. T2*-weighted echo planar images were collected for task-related fMRI (repetition time=2020ms, echo time= 50ms, flip angle=90°, voxel dimensions=3×3×3.5mm) and resting state fMRI (repetition time=1890ms, echo time=50ms, flip angle=90°, voxel dimensions=3×3×3.5mm). During the resting state scan, subjects were instructed to relax and think of nothing in particular. Three structural images were acquired: one T1-weighted structural scan in plane to the fMRI scans (repetition time=2000 ms; echo time=11ms; flip angle=150°; voxel dimensions=0.9×0.9×3.5 mm) and two T1-weighted volumetric magnetization prepared rapid gradient echo (MPRAGE) images (repetition time=2120 ms; echo time=3.58 ms; inversion time=1100 ms; flip angle=15°; voxel dimensions=1×1×1mm). MPRAGE images were averaged to obtain a high-quality structural image. T1-weighted images in plane to the fMRI data were used to improve coregistration of fMRI data to the

mean MPRAGE, which was used to normalize fMRI data to standard MNI space for group level analyses.

2.7 fMRI task

The setshift task was adapted from a design by Cools and colleagues (Cools et al., 2004). On each trial, a star and an hourglass appeared simultaneously on left and right sides of the computer screen; the location was counterbalanced. Bordering the star and hourglass was either a red or blue window. A blue window cued the subject to choose the target figure in the previous trial; if the target in the previous trial was a star, the correct answer was also a star. A red window cued the subject to choose the figure that was *not* a target in the previous trial; if the target in the previous trial was a star, the correct answer was an hourglass. The correct answer held true even if the subject made a wrong response. The first trial of every run included an arrow indicating the target figure. The subject began responding on the second trial. A red window followed by a blue window represented a shift: the rule changed. A red window followed by a red window represented a shift: the target figure changed. A blue window followed by a red window represented a shift; both the rule and the target figure changed. A blue window followed by a blue window represented no shift in rule or target figure (Fig. 2A).

Each subject performed 4 runs of 100 trials each. Each trial lasted 2950ms. On each trial, the stimulus appeared for 2000ms, during which the subject was instructed to make a response by pressing the response key in the left or right hand corresponding to the position of the target figure on the left or right side of the screen; the number of trials in which the target was on the left or right side of the screen was balanced so that each trial type had similar number of left and right hand responses. Feedback appeared after the stimulus for 500ms: a yellow happy face appeared if the response was correct, and a purple sad face appeared if the response was wrong. The subject was instructed to adjust his or her response according to the feedback. If the subject did not make a response within the 2000ms stimulus period, the purple sad face appeared, indicating that the response period had lapsed. A fixation cross appeared after the feedback, until the end of the trial. Each trial type had equal probability of appearing. Trial order was pseudorandomized such that no trial type appeared consecutively more than 3 times; the number of repeat trials was counterbalanced across trial type. Subjects practiced the task for 5 min before the experimental session commenced.

Response times from shift and no shift trials were averaged separately to form mean response times for each of the two trial types for each subject.

2.8 Task-related fMRI analysis

We used FSL for preprocessing and statistical analyses. Preprocessing included motion correction with MCFLIRT, brain extraction with BET, spatial smoothing with a 7mm full width half maximum Gaussian kernel, and high-pass temporal filtering (100s). Statistical analyses were performed using a general linear model implemented by FEAT. FILM prewhitening was applied to correct for temporal autocorrelation. Temporal derivatives and temporal filtering were included to improve fitting of the model to the data. Events were modeled at the time of stimulus presentation after convolution with a gamma hemodynamic

response function. In the first level analyses, for each subject and each scan, one regressor representing shift trials and one regressor representing no shift trials were modeled separately. Only correct trials were modeled. The feedback and fixation events were not modeled and thus functioned as the implicit baseline.

We decided to group all shift trial types in this analysis instead of investigating fMRI activity associated with shifts of object features and abstract rules individually because previous studies have shown that different forms of setshift engage the dopamine system differently (Cools et al., 2004). Since the focus of this manuscript is not to dissect the nuances of different forms of setshift but to understand relationships between COMT genotype, dopamine synthesis, resting state fMRI activity, task-related fMRI activity, and cognitive performance, we grouped all shift trial types to focus on brain areas commonly engaged by all types of setshift. Our findings on performance of object feature shift and abstract rule shift and their individual relationship to dopamine function were published previously (Dang et al., 2012a).

For group-level analyses, we first coregistered each functional scan to the T1-weighted structural image and then to the mean MPRAGE using 6 degrees of freedom rigid body transformations. The mean MPRAGE and its associated T1-weighted structural image and functional scans were normalized to MNI space using 12 degrees of freedom affine transformations. For each subject, first level results were combined in a paired t-test contrasting shift versus no shift trials. Subject-level results were averaged to obtain group-level contrast maps showing activation and deactivation during shift trials relative to no shift trials. Group-level contrast maps were thresholded at $z > 2.3$ with cluster thresholding to correct for multiple comparisons.

To identify brain regions related to setshift performance and dopamine function, we performed voxelwise analyses correlating group-level contrast maps with response time on shift trials and COMT genotype, represented by quadratic contrast coefficients. The results revealed that activity in the medial PFC is associated with both setshift performance and COMT genotype. We used the medial PFC cluster showing deactivation in the group-level contrast map as a region of interest from which to extract a mean deactivation value for each subject to correlate with other variables of interest. Mean deactivation values were calculated by averaging z-statistics extracted from subject-level maps using the medial PFC ROI.

2.9 Resting state fMRI analysis

To control for effects of scanner artifacts and physiological processes such as respiratory and cardiac functions, signal associated with the white matter, cerebrospinal fluid (CSF), and the global signal were entered as covariates in the regression of resting state fMRI data. To extract signal associated with white matter and CSF, each subject's mean MPRAGE was segmented into grey matter, white matter, and CSF using FSL-FAST. Signal intensity in CSF and white matter images was then thresholded at 90% and 99%, respectively, to ensure high tissue probability. Each individual's resting state fMRI scan was masked with the thresholded CSF and white matter images, and the mean time series was extracted for CSF

and white matter. Global signal was calculated by averaging across all voxels in the whole brain.

The removal of the global signal served two purposes in this study. The first purpose was to control for global effects common to all fMRI studies, such as scanner artifacts, gross body movement, and physiological processes. The second purpose was to control for effects of peripheral dopamine activity. Dopamine receptors are present in peripheral arteries, carotid bodies, and the endocrine system. Stimulation of these receptors has been found to affect vasodilation and myocardial contractility (Cavero et al., 1982). The global signal was removed to remove effects of peripheral dopamine from effects in the central nervous system.

The medial PFC is a component of the default mode network (DMN), a group of brain areas known to deactivate during task performance relative to baseline (Buckner et al., 2008). To explore the relationship between resting state and task-related activity, we calculated functional connectivity between the medial PFC and the DMN. Resting state fMRI scans were preprocessed in FSL using the following operations: motion correction with MCFLIRT, removal of non-brain matter with BET, spatial smoothing with a Gaussian kernel of 5 mm, and high-pass temporal filtering removing frequencies below 0.01Hz. We defined the DMN with a posterior cingulate (PCC) seed. Using the seed-based approach, Greicius and colleagues reported that peak connectivity in the PCC had MNI coordinates −2 −51 27 (Greicius et al., 2003). We generated an 8×8×8 mm^3 ROI around the peak connectivity voxel, coregistered the ROI to individual subject's resting state fMRI scan, and extracted the mean time series for voxels in the ROI mask. To extract the DMN mask, for each subject, we performed a regression in FSL-FEAT with the PCC mean time series and the three covariates discussed above. z-statistic maps from the regressions were averaged to generate the group-level DMN, which showed correlations between each voxel's time series and the PCC time series. To calculate functional connectivity between the medial PFC and the whole DMN for each subject, we coregistered the DMN mask to the resting state fMRI scan, extracted the mean times series for the whole DMN, and performed a regression with the DMN mean time series and the three covariates. The results were z-statistic maps showing correlations between each voxel's time series and the mean DMN time series. We extracted the mean z-statistic in the medial PFC using the identical ROI used to extract task-related deactivation. The mean z-statistic represented functional connectivity between the medial PFC and the DMN.

In addition to calculating functional connectivity from a DMN mask defined with a posterior cingulate seed, to confirm the results, we also calculated functional connectivity using a DMN mask extracted with independent component analysis. In addition to the 15 subjects in this study, we have resting state fMRI scans from an additional 13 subjects that participated in a different study in our lab but were recruited using the same criteria as this study; these 13 subjects were not included in other analyses in this study because they were not genotyped or did not perform the fMRI task. We performed independent component analysis on these 28 resting state fMRI scans and identified the component corresponding to the default mode network. Resting state fMRI scans were preprocessed as described above. Preprocessed scans were decomposed into separate spatial and temporal patterns using FSL-

MELODIC multi-session temporal concatenation. From the list of outputs, we identified the DMN as the component that has the most voxels overlapping with a DMN template from a previous study in the lab (Mormino et al., 2011). The spatial pattern corresponding to the DMN was coregistered to individual subject's resting state fMRI scan, and a mean time series for all voxels in the DMN mask was extracted for each subject from their preprocessed resting state scan. Functional connectivity was then calculated using the same approach as described above for the DMN mask defined with a posterior cingulate seed.

2.10 Statistics

Statistical tests were performed in R (Team, 2011). We used trend analyses to evaluate relationships between COMT, FMT, and functional connectivity. We used Pearson's correlations to relate resting state functional connectivity and task-related deactivation, and response time. FMT, functional connectivity, task-related deactivation, and response time were confirmed to be normally distributed using the Shapiro-Wilk normality test with an alpha of 0.05.

We used an automated variable selection method and bootstrap resampling to identify independent predictors of response time, task-related deactivation, and resting state functional connectivity. Automated variable selection methods are often used to identify independent predictors. However, the approach sometimes mistakenly identifies noise variables as independent predictors or yields models that are not reproducible. Bootstrapping repeatedly samples from the data to estimate the weight of evidence for a variable being an independent predictor. Validation of the approach found that selecting variables identified as independent predictors by at least 60% of the bootstrap samples yields an effective predictive model (Austin and Tu, 2004).

In the initial model, we included COMT, FMT, resting state functional connectivity, and task-related deactivation as predictors of response time. The method generated 1000 bootstrap samples from the dataset, used the Akaike information criterion to develop a parsimonious predictive model for each sample, and calculated the percentage of bootstrap samples in which a variable was identified as an independent predictor. In the next model, the variable identified as an independent predictor in the initial model became the outcome variable, and the other predictors in the initial model remained as predictors. The process continued until all independent predictors have been identified. Table 1 shows the models employed and the outcome independent predictors. Column 1 shows the input model. Column 2 shows the percent of bootstrap samples in which each variable appeared in the parsimonious model. Column 3 shows the independent predictor of that model or the variable that appeared in more than 60% of the bootstrap samples.

3. Results

3.1 Task-related fMRI activity

Relative to no-shift trials, setshift trials deactivated the medial PFC and posterior cingulate and activated the dorsolateral PFC and parietal lobule. Greater medial PFC deactivation correlated with faster response time during shift trials. Greater medial PFC deactivation was

also observed in Val/Met individuals relative to COMT homozygotes. There was no relationship between task-related activation and response time during shift trials or COMT genotype (Fig. 2B–D).

Greater deactivation in the medial PFC also correlated with faster response time during no shift trials (Pearson's r = 0.56, p-value = 0.029). Response times during no shift and shift trials were highly correlated (Pearson's r = 0.87, p-value = 2.0×10^{-5}). Given the collinearity, it was unclear whether the relationship between task-related fMRI activity and response time during no shift trials was dependent or independent of the relationship between response times during shift and no shift trials. To address the question of independent versus dependent effect, we used an automated variable selection method in conjunction with bootstrap resampling to identify independent predictors; results are shown below.

3.2 COMT and dopamine

Trend analyses showed that the number of Val alleles present correlated with increased FMT signal in the midbrain (Pearson's r = 0.62, p-value = 0.025), ventral striatum (Pearson's r = 0.70, p-value = 0.005), and putamen (Pearson's r = 0.62, p-value = 0.024). No significant correlation existed between COMT and FMT signal in the caudate (Pearson's r = 0.33, p-value = 0.808) (Fig. 1B–E).

3.3 Relationships with resting state functional connectivity

The DMN extracted with a posterior cingulate seed included the medial PFC, posterior cingulate, lateral parietal and left superior temporal cortices (Fig. 3A).

Greater medial PFC functional connectivity correlated with greater medial PFC deactivation during setshift performance (Pearson's r = 0.62, p-value = 0.013). Greater medial PFC functional connectivity also correlated with faster response time during shift trials (Pearson's r = 0.57, p-value = 0.028) (Fig. 3B–C). We used the automated variable selection method to determine whether the relationship between functional connectivity and performance was independent or dependent of the relationship between performance and task-related deactivation, with which functional connectivity was correlated (Pearson's r = 0.62, p-value = 0.013).

A trend analysis showed that Met/Val individuals had greater functional connectivity in the medial PFC than either Met/Met or Val/Val individuals (Pearson's r = 0.58, p-value = 0.030) (Fig. 3D).

Subjects were evenly divided into low, medium, and high FMT groups. Trend analyses showed that subjects with mid-range FMT values had higher functional connectivity than those with low or high FMT values in both the midbrain (Pearson's r = 0.63, p-value = 0.019) and ventral striatum (Pearson's r = 0.89, p-value = 1.4×10^{-4}). Correlations between functional connectivity and FMT values in the putamen (Pearson's r = 0.53, p-value = 0.056) and caudate (Pearson's r = 0.37, p-value = 0.222) were not significant (Fig. 3E–H).

To confirm that functional connectivity results were not affected by the approach with which we defined the DMN, we repeated these analyses using an independent components analysis method of defining the DMN, and all the significant relationships reported above remained (Fig. 4).

3.4 Automatic variable selection analysis

Figure 5A summarizes the significant correlations between COMT, FMT, functional connectivity, task-related deactivation, and response time. Figures 5B and 5C show the predictive models for response time during shift trials after elimination of dependent predictors when midbrain or ventral striatum FMT was in the model, respectively. Outputs from the automated variable selection method are presented in Table 1. Results did not differ whether functional connectivity was calculated from the DMN defined with a posterior cingulate seed or extracted by independent component analysis. For predicting response time during shift trials, task-related fMRI activity was the independent predictor of response time, and functional connectivity was the independent predictor of task-related fMRI activity. COMT and FMT were both independent predictors of functional connectivity when midbrain FMT was in the model. When ventral striatum FMT replaced midbrain FMT in the model, ventral striatum FMT was the only predictor of functional connectivity, and COMT was the predictor of ventral striatum FMT. No independent predictor was identified for response time during no shift trials.

4. Discussion

Genetic effects on behavior are undoubtedly mediated by a host of biochemical and physiological processes. We studied the downstream processes whereby the COMT gene influences prefrontal cognition. We performed fMRI with a setshift task to identify brain areas associated with cognitive flexibility, a function previously shown to engage the prefrontal cortex and the dopamine system (Cools et al., 2004; Monchi et al., 2006). We found that setshift performance deactivated the medial PFC and posterior cingulate, two nodes in the DMN (Buckner et al., 2008; Raichle et al., 2001). Setshift performance also activated the dorsolateral PFC and parietal lobule; these areas form the frontoparietal control network, which consistently activates during performance of tasks probing the prefrontal cortex (Vincent et al., 2008). The deactivation and activation profile of the setshift task resembles results from previous fMRI studies of prefrontal function, assuring us that the setshift task engaged brain regions involved in prefrontal cognition (Chee and Choo, 2004).

We found that greater deactivation in the medial PFC correlated with faster response time during shift trials. The DMN is believed to support a variety of internal mental processes. In studies of spontaneous internal cognition, subjects with frequent mindwandering show higher DMN activity (Mason et al., 2007). In tasks where mindwandering is suppressed in favor of focused attention on external cues, the DMN consistently deactivates (Buckner et al., 2008). Our result supports the hypothesis that optimal task performance involves successful reallocation of attentional resources from the DMN to areas involved in task performance, such as the fronto-parietal control network (McKiernan et al., 2003). Furthermore, the DMN is hypothesized to comprise two subsystems: a medial temporal lobe

subsystem that facilitates memory retrieval and a medial PFC subsystem that simulates interactions between retrieved memories (Buckner et al., 2008). Performance of the setshift task requires greater attention to forming associations between task cues than retrieving long term memory. The relationship between medial PFC deactivation and setshift performance suggests that subsystems of the DMN have independent roles and that cognitive flexibility preferentially involves the medial PFC subsystem.

Response time during shift trials did not correlate with COMT genotype. Although task performance has been associated with COMT, the immediate function of COMT is dopamine degradation, suggesting that the direct effect of COMT is on dopaminergic function. We found that FMT signal in the midbrain, ventral striatum, and putamen increased with the number of Val alleles, consistent with a previous study that employed PET with [18F]fluorodopa and found that Val carriers had greater dopamine synthesis than Met homozygotes (Meyer-Lindenberg et al., 2005). Dopamine activity is regulated by multiple feedback mechanisms in the dopamine system. For instance, lower dopamine receptor density is offset by greater dopamine synthesis capacity (Laakso et al., 2005), and effects of excessive receptor stimulation are negated by receptor desensitization (Cooper et al., 2003). Our findings suggest that individuals with the Val allele show greater dopamine synthesis. This may represent, in part, compensation for lower dopamine concentration in the PFC.

Dopamine has been proposed to enhance the neural response by suppressing noisy spontaneous activity from neurons (Grace, 2000). Electrophysiological recordings in monkeys found that stimulation of dopamine receptors reduces the width of tuning curves of prefrontal neurons and suppresses responses to nonpreferred directions in a spatial working memory task, resulting in better memory performance (Vijayraghavan et al., 2007). Local field potential recordings found that dopamine increases neuronal synchrony in frequencies associated with cognitive functions (Brown, 2003), perhaps by tuning the response curve of disparate neurons to the relevant frequency band. fMRI may capture dopaminergic modulation of neuronal synchrony via functional connectivity in RSNs. Functional connectivity has been shown to be highly susceptible to manipulation of endogenous dopamine level. Dopamine agonists increase functional connectivity (Kelly et al., 2009) while dopamine depletion reduces functional connectivity and its relationship to cognitive performance (Nagano-Saito et al., 2008). Our finding of a relationship between endogenous dopamine activity and functional connectivity encourages future studies to investigate neuronal synchrony as a possible cellular mechanism for functional connectivity.

Specifically, we found an inverted-U relationship whereby subjects with mid-range FMT values had significantly higher functional connectivity than those with low or high FMT values. These relationships were present in the midbrain and the ventral striatum but not the caudate or putamen. Dopaminergic neurons in the midbrain are localized in the substantia nigra and the ventral tegmentum. Because nigral neurons project to dorsal caudate and putamen, and ventral tegmental neurons project to the ventral striatum and PFC, our results suggest that it is the ventral tegmental system, and thus the mesocortical and mesolimbic systems that are involved in these relationships.

We also found that Met/Val individuals, who had mid-range dopamine synthesis, had greater functional connectivity than both Met/Met individuals who had low dopamine synthesis and Val/Val individuals who had high dopamine synthesis. Both COMT and FMT were identified as independent predictors of functional connectivity by the automated variable selection method when midbrain FMT was in the model, suggesting that COMT also influences functional connectivity by a mechanism that we did not measure, such as dopamine release or receptor behavior. When ventral striatum FMT replaced midbrain FMT in the model, ventral striatum FMT was identified as the only predictor of functional connectivity, and COMT was the predictor of ventral striatum FMT. Midbrain FMT reflects the synthesis capacity of the whole dopamine system whereas ventral striatum FMT reflects the mesocorticolimbic pathway. These results suggest that the mesocorticolimbic pathway dominates effects on functional connectivity and COMT effects become less visible. These dynamics between dopamine synthesis and its distribution in the different pathways deserve further investigation in future studies.

The relationship between dopamine and a variety of neural and behavioral responses has previously been characterized as an inverted-U shape (Dickinson and Elvevag, 2009), indicating that optimal dopamine levels result in maximum efficiency in the PFC. Deviations from the optimal level toward the low or high ends both result in decreased efficiency. Support for the inverted-U hypothesis has come from studies manipulating endogenous dopamine level. In humans, administration of dopamine agonists improve performance in individuals with low endogenous dopamine level but impairs performance in those with high endogenous dopamine level (Mattay et al., 2003). In monkeys, both too much and too little stimulation of dopamine receptors in the prefrontal cortex impairs performance (Vijayraghavan et al., 2007). Our results suggest that both COMT genotype and dopamine synthesis are associated with an inverted-U function that is instantiated in the brain at the level of the prefrontal components of a resting-state default mode network.

Furthermore, we found that functional connectivity correlated with task-related deactivation in the medial PFC. Several studies have remarked on the similarities between RSNs and patterns of task-induced activity and suggested that RSNs reflect functional networks in their idling state (Mennes et al., 2010; Smith et al., 2009; Thomason et al., 2008). Our results support the hypothesis that the integrity of functional networks at “rest”, as measured by functional connectivity, determines the ability of the network to perform the task, as measured by task-related fMRI (De Luca et al., 2006). We also found a correlation between functional connectivity and response time during shift trials. Resting state functional connectivity has been directly correlated with behavioral performance (Nagano-Saito et al., 2008). However, functional connectivity was not identified as an independent predictor of performance by the automated variable selection method, suggesting that the relationship between functional connectivity and performance stems from the relationship between performance and task-related fMRI activity, with which functional connectivity is correlated.

The integration of our results through the models in Fig. 5B and C demonstrates that COMT modulates dopamine synthesis, which supports functional connectivity in resting state networks in an inverted-U pattern. COMT may also influence functional connectivity in the

same pattern by a mechanism independent of dopamine synthesis. Functional connectivity affects task-related deactivation, which modulates performance of prefrontal functions. These results form a model for the mechanisms whereby genetic drivers of dopamine synthesis modulate a system in which intermediate levels of dopaminergic function result in optimal performance.

In this study, changes in BOLD activity were observed in both the default mode network and the fronto-parietal control network during setshift performance, but the relationship between performance and BOLD activity was only found in the default mode network. Previous studies assessing prefrontal functions have also associated BOLD activity in the fronto-parietal control network with performance (Klingberg et al., 1997; Naghavi and Nyberg, 2005). Currently it is not clear how the default mode network and the fronto-parietal control function together to modulate cognition. Spreng and colleagues showed that activities in the fronto-parietal control network and the default mode network are coupled during internally driven cognition and uncoupled during externally driven cognition (Spreng et al., 2010). Vincent and colleagues observed that the fronto-parietal control network is anatomically adjacent to both the default mode network and the dorsal attention network, leading them to propose that the fronto-parietal control network flexibly couples to the default mode network or the dorsal attention network depending on the current cognitive task (Vincent et al., 2008). More research is needed to determine whether the default mode network and the fronto-parietal control network are equal partners in influencing cognition or that one network is secondary to the other. Furthermore, dopamine has not only been associated with the fronto-parietal control network (Landau et al., 2009; Tan et al., 2007; Wimber et al., 2011) but also with the degree of coupling between this network and the default mode network (Dang et al., 2012b). It is not known whether dopamine affects the default mode network and the fronto-parietal control network equally or that dopamine plays a direct role in one network, and since the two networks are related, dopamine also correlates with activity in the other network. It is also possible that the role of dopamine in these two networks varies with the task. This study assessed the role of dopamine in setshifting, and it remains to be investigated whether our findings can be generalized to other executive functions. Future studies should investigate not only how dopamine affects the default mode network and the fronto-parietal control network individually but also how the fronto-parietal control network and the default mode network interact to affect cognition and the role of dopamine in this interaction.

One limitation of this study is the small sample size. However, for any correlation presented in the manuscript that is not a replication of previous findings, we analyzed the data using more than one approach to confirm the results. Our genotype results are entirely consistent with previous post-mortem and *in vivo* reports (Akil et al., 2003; Meyer-Lindenberg et al., 2005). We also observed the relationship between COMT genotype and FMT uptake in multiple ROIs, in both the midbrain and the striatum. It is possible, if the results were spurious, to detect the relationship between FMT uptake and COMT genotype in one ROI, but the finding is much less likely to be replicated in multiple ROIs. Furthermore, we replicated our findings with resting state functional connectivity by defining the default mode network using two separate approaches.

In summary, dopamine has been proposed to perform a gating function allowing or blocking afferent information into the prefrontal cortex, thus modulating attention (Montague et al., 2004). Also involved in attention, the DMN deactivates to reallocate processing resources from self- referential to external goal-directed behavior (Buckner et al., 2008). Patients with dopamine disorders exhibit not only DMN disconnection but also deficits on tasks requiring attention to shift between existing and incoming information (Cools et al., 2001; van Eimeren et al., 2009), suggesting that dopamine modulates attention via the DMN. Our results support the role of dopamine in this system and show that genetic factors affect dopamine synthesis, which in turn affect the resting state and brain activation in the anterior medial prefrontal cortex component of this network.

Acknowledgments

This research was supported by NIH grant AG027984.

6. References

Akil M, Kolachana BS, Rothmond DA, Hyde TM, Weinberger DR, Kleinman JE. Catechol-O-methyltransferase genotype and dopamine regulation in the human brain. J Neurosci. 2003; 23:2008–2013. [PubMed: 12657658]

Austin PC, Tu JV. Bootstrap Methods for Developing Predictive Models. The American Statistician. 2004; 58:7.

Biswal B, Yetkin FZ, Haughton VM, Hyde JS. Functional connectivity in the motor cortex of resting human brain using echo-planar MRI. Magn Reson Med. 1995; 34:537–541. [PubMed: 8524021]

Braver TS, Cohen JD. On the Control of Control: The Role of Dopamine in Regulating Prefrontal Function and Working Memory. Control of Cognitive Processes. 2000:713–736.

Brown P. Oscillatory nature of human basal ganglia activity: relationship to the pathophysiology of Parkinson's disease. Mov Disord. 2003; 18:357–363. [PubMed: 12671940]

Buckner RL, Andrews-Hanna JR, Schacter DL. The brain's default network: anatomy, function, and relevance to disease. Ann N Y Acad Sci. 2008; 1124:1–38. [PubMed: 18400922]

Cavero I, Massingham R, Lefevre-Borg F. Peripheral dopamine receptors, potential targets for a new class of antihypertensive agents. Part I: Subclassification and functional description. Life Sci. 1982; 31:939–948. [PubMed: 6752615]

Chee MW, Choo WC. Functional imaging of working memory after 24 hr of total sleep deprivation. J Neurosci. 2004; 24:4560–4567. [PubMed: 15140927]

Clark WG, Oldendorf WH, Dewherst WG. Blood-brain barrier to carbidopa (MK-486) and Ro 4-4602, peripheral dopa decarboxylase inhibitors. J Pharm Pharmacol. 1973; 25:416–418. [PubMed: 4146401]

Cools R, Barker RA, Sahakian BJ, Robbins TW. Mechanisms of cognitive set flexibility in Parkinson's disease. Brain. 2001; 124:2503–2512. [PubMed: 11701603]

Cools R, Clark L, Robbins TW. Differential responses in human striatum and prefrontal cortex to changes in object and rule relevance. J Neurosci. 2004; 24:1129–1135. [PubMed: 14762131]

Cooper, JR.; Bloom, FE.; Roth, RH. The biochemical basis of neuropharmacology. 8th ed.. Oxford University Press; Oxford; New York: 2003.

Dang LC, Donde A, Madison C, O'Neil JP, Jagust WJ. Striatal Dopamine Influences the Default Mode Network to Affect Shifting between Object Features. J Cogn Neurosci. 2012a

Dang LC, O'Neil JP, Jagust WJ. Dopamine supports coupling of attention-related networks. J Neurosci. 2012b; 32:9582–9587. [PubMed: 22787044]

De Luca M, Beckmann CF, De Stefano N, Matthews PM, Smith SM. fMRI resting state networks define distinct modes of long-distance interactions in the human brain. Neuroimage. 2006; 29:1359–1367. [PubMed: 16260155]

DeJesus OT. Positron-Labeled DOPA Analogs to Image Dopamine Terminals. Drug Development Research. 2003; 59:11.

Dickinson D, Elvevag B. Genes, cognition and brain through a COMT lens. Neuroscience. 2009; 164:72–87. [PubMed: 19446012]

Egan MF, Goldberg TE, Kolachana BS, Callicott JH, Mazzanti CM, Straub RE, Goldman D, Weinberger DR. Effect of COMT Val108/158 Met genotype on frontal lobe function and risk for schizophrenia. Proc Natl Acad Sci U S A. 2001; 98:6917–6922. [PubMed: 11381111]

Folstein MF, Folstein SE, McHugh PR. “Mini-mental state”. A practical method for grading the cognitive state of patients for the clinician. J Psychiatr Res. 1975; 12:189–198. [PubMed: 1202204]

Grace AA. The tonic/phasic model of dopamine system regulation and its implications for understanding alcohol and psychostimulant craving. Addiction. 2000; 95(Suppl 2):S119–128. [PubMed: 11002907]

Greicius MD, Krasnow B, Reiss AL, Menon V. Functional connectivity in the resting brain: a network analysis of the default mode hypothesis. Proc Natl Acad Sci U S A. 2003; 100:253–258. [PubMed: 12506194]

Kelly C, de Zubicaray G, Di Martino A, Copland DA, Reiss PT, Klein DF, Castellanos FX, Milham MP, McMahon K. L-dopa modulates functional connectivity in striatal cognitive and motor networks: a double-blind placebo-controlled study. J Neurosci. 2009; 29:7364–7378. [PubMed: 19494158]

Klingberg T, O'Sullivan BT, Roland PE. Bilateral activation of fronto-parietal networks by incrementing demand in a working memory task. Cereb Cortex. 1997; 7:465–471. [PubMed: 9261575]

Laakso A, Pohjalainen T, Bergman J, Kajander J, Haaparanta M, Solin O, Syvalahti E, Hietala J. The A1 allele of the human D2 dopamine receptor gene is associated with increased activity of striatal L-amino acid decarboxylase in healthy subjects. Pharmacogenet Genomics. 2005; 15:387–391. [PubMed: 15900211]

Lachman HM, Papolos DF, Saito T, Yu YM, Szumlanski CL, Weinshilboum RM. Human catechol-O-methyltransferase pharmacogenetics: description of a functional polymorphism and its potential application to neuropsychiatric disorders. Pharmacogenetics. 1996; 6:243–250. [PubMed: 8807664]

Landau SM, Lal R, O'Neil JP, Baker S, Jagust WJ. Striatal dopamine and working memory. Cereb Cortex. 2009; 19:445–454. [PubMed: 18550595]

Mason MF, Norton MI, Van Horn JD, Wegner DM, Grafton ST, Macrae CN. Wandering minds: the default network and stimulus-independent thought. Science. 2007; 315:393–395. [PubMed: 17234951]

Mattay VS, Goldberg TE, Fera F, Hariri AR, Tessitore A, Egan MF, Kolachana B, Callicott JH, Weinberger DR. Catechol O-methyltransferase val158-met genotype and individual variation in the brain response to amphetamine. Proc Natl Acad Sci U S A. 2003; 100:6186–6191. [PubMed: 12716966]

Mawlawi O, Martinez D, Slifstein M, Broft A, Chatterjee R, Hwang DR, Huang Y, Simpson N, Ngo K, Van Heertum R, Laruelle M. Imaging human mesolimbic dopamine transmission with positron emission tomography: I. Accuracy and precision of D(2) receptor parameter measurements in ventral striatum. J Cereb Blood Flow Metab. 2001; 21:1034–1057. [PubMed: 11524609]

McKiernan KA, Kaufman JN, Kucera-Thompson J, Binder JR. A parametric manipulation of factors affecting task-induced deactivation in functional neuroimaging. J Cogn Neurosci. 2003; 15:394–408. [PubMed: 12729491]

Mennes M, Kelly C, Zuo XN, Di Martino A, Biswal B, Castellanos FX, Milham MP. Inter-individual differences in resting state functional connectivity predict task-induced BOLD activity. Neuroimage. 2010

Meyer-Lindenberg A, Kohn PD, Kolachana B, Kippenhan S, McInerney-Leo A, Nussbaum R, Weinberger DR, Berman KF. Midbrain dopamine and prefrontal function in humans: interaction and modulation by COMT genotype. Nat Neurosci. 2005; 8:594–596. [PubMed: 15821730]

Monchi O, Ko JH, Strafella AP. Striatal dopamine release during performance of executive functions: A [(11)C] raclopride PET study. Neuroimage. 2006; 33:907–912. [PubMed: 16982202]

Monchi O, Petrides M, Doyon J, Postuma RB, Worsley K, Dagher A. Neural bases of set-shifting deficits in Parkinson's disease. J Neurosci. 2004; 24:702–710. [PubMed: 14736856]

Montague PR, Hyman SE, Cohen JD. Computational roles for dopamine in behavioural control. Nature. 2004; 431:760–767. [PubMed: 15483596]

Mormino EC, Smiljic A, Hayenga AO, Onami SH, Greicius MD, Rabinovici GD, Janabi M, Baker SL, Yen IV, Madison CM, Miller BL, Jagust WJ. Relationships between beta-amyloid and functional connectivity in different components of the default mode network in aging. Cereb Cortex. 2011; 21:2399–2407. [PubMed: 21383234]

Nagano-Saito A, Leyton M, Monchi O, Goldberg YK, He Y, Dagher A. Dopamine depletion impairs frontostriatal functional connectivity during a set-shifting task. J Neurosci. 2008; 28:3697–3706. [PubMed: 18385328]

Naghavi HR, Nyberg L. Common fronto-parietal activity in attention, memory, and consciousness: shared demands on integration? Conscious Cogn. 2005; 14:390–425. [PubMed: 15950889]

Nolan KA, Bilder RM, Lachman HM, Volavka J. Catechol O-methyltransferase Val158Met polymorphism in schizophrenia: differential effects of Val and Met alleles on cognitive stability and flexibility. Am J Psychiatry. 2004; 161:359–361. [PubMed: 14754787]

Patlak CS, Blasberg RG. Graphical evaluation of blood-to-brain transfer constants from multiple-time uptake data. Generalizations. J Cereb Blood Flow Metab. 1985; 5:584–590. [PubMed: 4055928]

Raichle ME, MacLeod AM, Snyder AZ, Powers WJ, Gusnard DA, Shulman GL. A default mode of brain function. Proc Natl Acad Sci U S A. 2001; 98:676–682. [PubMed: 11209064]

Sharott A, Magill PJ, Harnack D, Kupsch A, Meissner W, Brown P. Dopamine depletion increases the power and coherence of beta-oscillations in the cerebral cortex and subthalamic nucleus of the awake rat. Eur J Neurosci. 2005; 21:1413–1422. [PubMed: 15813951]

Smith SM, Fox PT, Miller KL, Glahn DC, Fox PM, Mackay CE, Filippini N, Watkins KE, Toro R, Laird AR, Beckmann CF. Correspondence of the brain's functional architecture during activation and rest. Proc Natl Acad Sci U S A. 2009; 106:13040–13045. [PubMed: 19620724]

Spreng RN, Stevens WD, Chamberlain JP, Gilmore AW, Schacter DL. Default network activity, coupled with the frontoparietal control network, supports goal-directed cognition. Neuroimage. 2010; 53:303–317. [PubMed: 20600998]

Tan HY, Chen Q, Goldberg TE, Mattay VS, Meyer-Lindenberg A, Weinberger DR, Callicott JH. Catechol-O-methyltransferase Val158Met modulation of prefrontal-parietal-striatal brain systems during arithmetic and temporal transformations in working memory. J Neurosci. 2007; 27:13393–13401. [PubMed: 18057197]

Team, RDC. R: A language and environment for statistical computing. R Foundation for Statistical Computing; Vienna, Austria: 2011.

Thomason ME, Chang CE, Glover GH, Gabrieli JD, Greicius MD, Gotlib IH. Default-mode function and task-induced deactivation have overlapping brain substrates in children. Neuroimage. 2008; 41:1493–1503. [PubMed: 18482851]

van Eimeren T, Monchi O, Ballanger B, Strafella AP. Dysfunction of the default mode network in Parkinson disease: a functional magnetic resonance imaging study. Arch Neurol. 2009; 66:877–883. [PubMed: 19597090]

VanBrocklin HF, Blagoev M, Hoepping A, O'Neil JP, Klose M, Schubiger PA, Ametamey S. A new precursor for the preparation of 6-[18F]Fluoro-L-m-tyrosine ([18F]FMT): efficient synthesis and comparison of radiolabeling. Appl Radiat Isot. 2004; 61:1289–1294. [PubMed: 15388123]

Vijayraghavan S, Wang M, Birnbaum SG, Williams GV, Arnsten AF. Inverted-U dopamine D1 receptor actions on prefrontal neurons engaged in working memory. Nat Neurosci. 2007; 10:376–384. [PubMed: 17277774]

Vincent JL, Kahn I, Snyder AZ, Raichle ME, Buckner RL. Evidence for a frontoparietal control system revealed by intrinsic functional connectivity. J Neurophysiol. 2008; 100:3328–3342. [PubMed: 18799601]

Ward LM. Synchronous neural oscillations and cognitive processes. Trends Cogn Sci. 2003; 7:553–559. [PubMed: 14643372]

Wimber M, Schott B, Wendler F, Seidenbecher C, Behnisch G, Macharadze T, Bauml K, Richardson-Klavehn A. Prefrontal dopamine and the dynamic control of human long-term memory. Translational Psychiatry. 2011; 1

Web References

FMRI Software Library. http://www.fmrib.ox.ac.uk/fsl/. Last visited 8/20/2011

R.. http://www.r-project.org/. Last visited 8/20/2011

Highlights

COMT genotype determines dopamine synthesis.

Dopamine synthesis influences resting state functional connectivity.

Functional connectivity correlates positively with task-related deactivation.

Greater deactivation is associated with better cognitive performance.

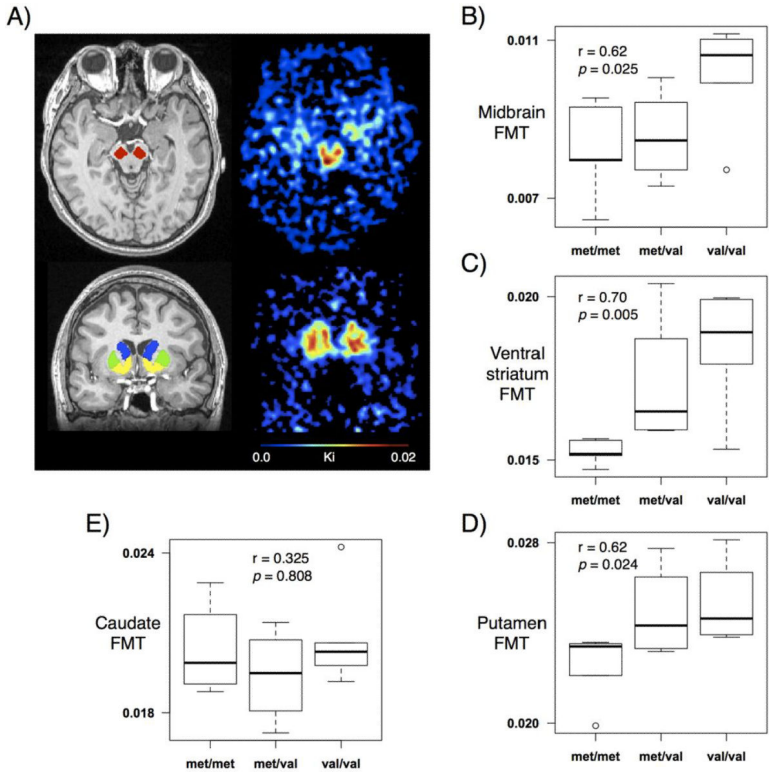

Fig 1.

Regions of interest. A) Examples from one subject. Left column shows midbrain (red), caudate (blue), putamen (green), and ventral striatum (yellow) ROIs superimposed on the mean MPRAGE. Right column shows FMT uptake in the midbrain and striatum. B–D) FMT uptake in the midbrain, ventral striatum, and putamen increased as the number of Val alleles increased. E) No relationship between COMT and FMT uptake in the caudate.

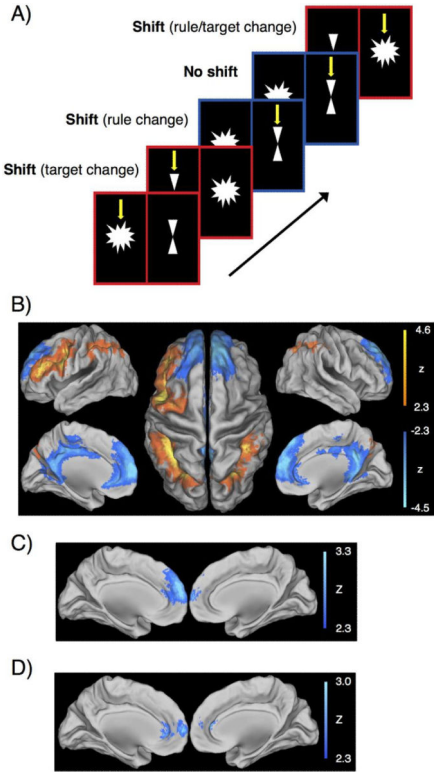

Fig 2.

Performance of the setshift task. A) Schematic of the task showing shift and no shift trials. Yellow arrows indicate the correct answer for each trial. B) Voxelwise analysis contrasting shift minus no shift trials found activation (orange) in the left PFC and bilateral parietal lobule and deactivation (blue) in the medial PFC (mPFC) and posterior cingulate. C) Greater deactivation in the mPFC correlated with faster response time (RT) during shift trials. D) Greater deactivation in the mPFC was also observed in Val/Met individuals relative to COMT homozygotes.

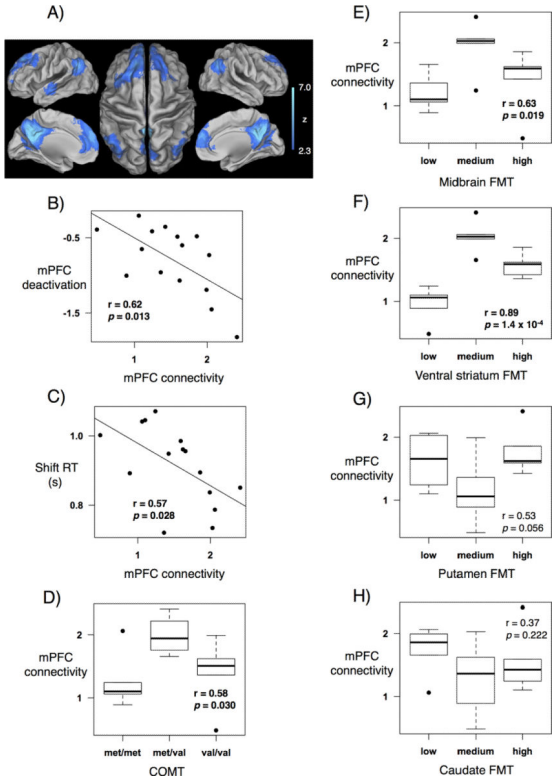

Fig 3.

Relationships with functional connectivity. A) Default mode network, extracted with a posterior cingulate/precuneus seed, included the medial PFC, posterior cingulate/precuneus, lateral parietal and superior temporal areas. B) Greater mPFC functional connectivity correlated with greater mPFC deactivation. C) Greater mPFC functional connectivity correlated with faster RT during shift trials. D–F) Inverted-U relationships between mPFC functional connectivity and COMT, midbrain FMT, and ventral striatum FMT. G–H) Relationships between mPFC functional connectivity and caudate and putamen FMT were not significant.

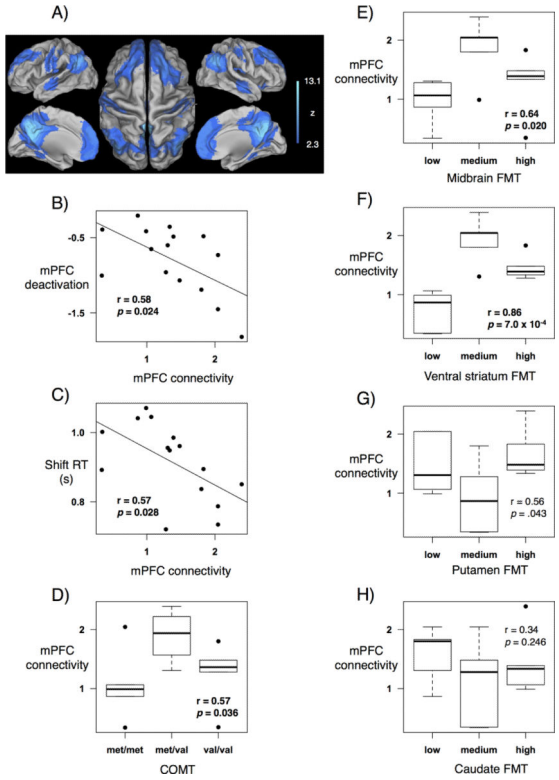

Fig 4.

Functional connectivity results replicated. The DMN mask extracted with independent component analysis yielded similar functional connectivity results as the DMN mask defined with a posterior cingulate seed.

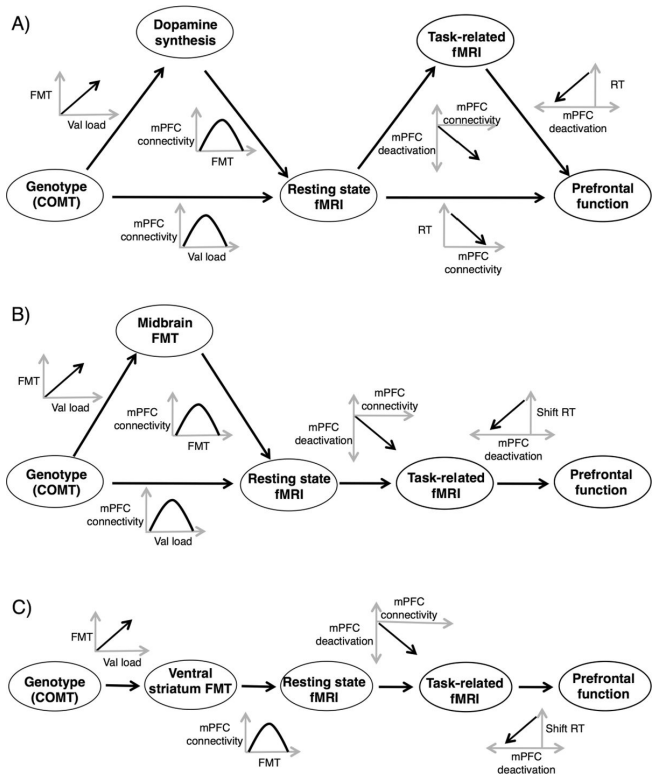

Fig 5.

Correlation diagrams. A) Correlations between COMT, FMT, resting state fMRI activity, task-related fMRI activity, and response time. Next to each arrow connecting 2 correlated variables are plots showing the direction and shape of the correlation. B) Predictive model with midbrain FMT after elimination of dependent predictors. C) Predictive model with ventral striatum FMT after elimination of dependent predictors. In all diagrams, negative values for mPFC deactivation (south on the y-axis or left on the x-axis) reflect greater deactivation in the medial PFC.

Table 1

Identification of independent predictors for response time, task-related fMRI activity, and functional connectivity (FC). Independent predictors for each model were variables identified as predictors in more than 60% of the bootstrapped samples. This table shows the percentage of bootstrapped samples in which each variable was identified as a predictor in each model. Column 1 shows the initial model with the outcome variable and its predictors. Column 2 shows the percentage of bootstrap samples, out of 1000 samples, that each predictor was selected in the parsimonious model, the outcome model of the automated variable selection method. Column 3 shows the independent predictor identified by being selected in more than 60% of the bootstrap samples. For predicting RT during shift trials when midbrain FMT was in the model, a) task-related fMRI activity was the independent predictor of RT, b) FC was the independent predictor of task-related fMRI activity, and c) COMT and FMT were independent predictors of FC. These results are summarized in Fig. 4B. For predicting RT during shift trials when ventral striatum FMT was in the model, a) task-related fMRI activity was the independent predictor of RT, b) FC was the independent predictor of task-related fMRI activity, c) FMT was the independent predictor of FC, and d) COMT was the predictor of FMT. These results are summarized in Fig. 4C. No variable was identified as an independent predictor of response time during no shift trials.

Identification of independent predictors by the automated variable selection method and bootstrap resampling		
Initial model	**% bootstrap samples**	**Independent predictor**
1) Predicting shiftRT with midbrain FMT		
shift RT = task fMRI + FC + midbrain FMT + COMT	task fMRI = 70.9	task fMRI
	FC = 34.1	
	FMT = 40.9	
	COMT = 40.7	
task fMRI = FC + midbrain FMT + COMT	FC = 75.9	FC
	FMT = 37.6	
	COMT = 45.4	
FC = midbrain FMT + COMT	FMT = 88.3	FMT, COMT
	COMT = 88.8	
2) Predicting no shift RT with midbrain FMT		
no shift RT = task fMRI + FC + midbrain FMT + COMT	task fMRI = 58.4	no independent predictor selected
	FC = 29.4	
	FMT = 49.4	
	COMT = 57.9	
3) Predicting shift RT with ventral striatum FMT		
shift RT = task fMRI + FC + ventral striatum FMT + COMT	task fMRI = 71.6	task fMRI
	FC = 28.2	
	FMT = 36.9	
	COMT = 37.0	
task fMRI = FC + ventral striatum FMT + COMT	FC = 67.8	FC
	FMT = 56.7	
	COMT =55.9	

Identification of independent predictors by the automated variable selection method and bootstrap resampling		
Initial model	**% bootstrap samples**	**Independent predictor**
FC = ventral striatum FMT + COMT	FMT = 91.38	FMT
	COMT = 54.44	
4) Predicting no shift RT with ventral striatum FMT		
no shift RT = task fMRI + FC + ventral striatum FMT + COMT	task fMRI = 53.5	no independent predictor selected
	FC = 25.8	
	FMT =55.6	
	COMT = 44.0	